Cerebral vessel segmentation in CE-MR images using deep learning and synthetic training datasets

Artur Klepaczko

Institute of Electronics, Lodz University of Technology, Łódź, Poland,
artur.klepaczko@p.lodz.pl

Abstract. This paper presents a novel architecture of a convolutional neural network designed for the segmentation of intracranial arteries in contrast-enhanced magnetic resonance angiography (CE-MRA). The proposed architecture is based on the V-Net model, however, with substantial modifications in the bottleneck and the decoder part. In order to leverage multiscale characteristics of the input vessel patterns, we postulate to pass the network embeddings generated on the encoder path output through the atrous spatial pyramid pooling block. We motivate that this mechanism allows the decoder part to rebuild the segmentation mask based on local features, however, determined at various ranges of voxels neighborhoods. The ASPP outputs are aggregated using a simple gated recurrent unit which, on the other hand, facilitates the learning of feature maps' relevance with respect to the final output. We also propose to enrich the global context information provided to the decoder by including a vessel-enhancement block responsible for filtering out background tissues. In this study, we also aimed to verify if it is possible to train an effective deep-learning vessel segmentation model based solely on synthetic data. For that purpose, we reconstructed 30 realistic cerebral arterial tree models and used our previously developed MRA simulation framework.

Keywords: Vessel segmentation · Cerebral arterial models · Contrast-Enhanced MR angiography · MR angiography simulation.

1 Introduction

Vessel segmentation is a key step in the analysis of angiographic images. It allows the reconstruction and visualization of the topology of the vascular system of body organs and helps to detect anatomical malformations such as stenoses, occlusions, or aneurysms. One of the routinely used techniques in the diagnosis of cerebral vessels is contrast-enhanced magnetic resonance angiography (CE-MRA). This method requires the application of a gadolinium-based contrast agent injected intravenously as a bolus, i.e. a dose of the agent with a volume of several to 20 ml administered over a short period of time. In the ionized state, gadolinium is a paramagnetic medium, which effectively shortens the T_1

ICCS Camera Ready Version 2023
To cite this paper please use the final published version:
DOI: 10.1007/978-3-031-36027-5_20

relaxation time of the penetrated body fluids and tissues. Although gadolinium itself is toxic, its clinically used form is *chelated*, which means that a Gd^{3+} ion is bound by a molecular cage giving the agent the required safety profile. An advantage of CE-MRI in comparison with non-contrast techniques, such as Time-of-Flight (ToF) or Phase Contrast Angiography (PCA), is that the former provides excellent contrast of the vessels with respect to other tissues, is free from or less pronounced to flow- and motion-related artifacts and allows good separation of the signal from arteries and veins. The latter is achieved by proper configuration of scanning times so that the signal is acquired at peak concentration of the agent bolus in the arteries before it reaches the capillary bed during its passage through the vascular system. Moreover, CE-MRA does not suffer from other artifactual signal loss mechanisms characteristic of ToF and PCA, such as intra-voxel dephasing and blood spins saturation due to slow, in-plane, recirculating blood flow. On the drawbacks side, one must note that CE-MRI is not recommended in patients with severe renal impairment or after kidney replacement therapy, and in those who may develop a hypersensitive reaction to the gadolinium agent. The risk factors of the latter include multiple allergies, asthma, and a history of hypersensitive reactions to gadolinium and iodinated contrast agents.

This paper focuses on CE-MRA in application to the imaging of cerebral arteries. It must be noted that each imaging modality (such as MRI and computed tomography, e.g.) and a specific method within a given modality (like ToF and CE-MRA) possess characteristic intensity patterns, both with respect to vessels and the surrounding tissues. Hence, machine-learning-based vessel segmentation methods, which rely not only on geometrical features describing tubular elongated shapes of arteries and veins but also on the texture information related to the vessels' lumen and surrounding context, must be developed on the training data corresponding to the target modality. There can be two cases distinguished in regard to the availability of training examples. If there are sufficient images, then the development of semantic segmentation models is conceptually straightforward. On the other hand, when the training images of the target modality are scarce, one could use transfer learning—first, pre-train the model using, e.g. CT data and then fine-tune it with a relatively smaller set of MR images. In any case, the most tedious work is the data annotation so that the model can learn how to differentiate vessel pixels (or voxels in 3D) from background tissues.

In order to avoid the effort of manual data annotation, some researchers use synthetically generated vessel trees. The geometrical tree models are converted into images and ground-truth annotations. Usually, these images are oversimplified, both in terms of specific patterns characteristic of a given imaging modality and the complexity of the vessel system. Hence, the reliability of such models is limited to cases consisting of only a few straight large-scale branches, such as e.g. carotid arteries. Therefore the goal of this work is to show that it is possible to develop a deep-learning multi-scale vessel segmentation model ensuring state-of-the-art performance using the simulated CE-MRA images reconstructed for the realistic arterial tree models. The details of our concept are provided in the

ICCS Camera Ready Version 2023
To cite this paper please use the final published version:
DOI: 10.1007/978-3-031-36027-5_20

subsequent sections as follows. In Sect. 2, we give a summary of the published works concerning vessel segmentation, giving focus on deep-learning technology. This section completes with a list of contributions of our study in light of the presented SOTA methods. Section 3 presents the proposed architecture of a neural network dedicated to the segmentation of multi-scale vessel structures. Then we describe the developed framework for CE-MRA image synthesis which is based on our previous achievements in non-contrast MRA simulations. The results of experiments are presented in Sect. 4, and finally, Sect. 5 concludes.

2 Related work

2.1 State-of-the-art methods

The importance of the vessel segmentation problem in the analysis of angiographic images resulted in numerous contributions over the last two decades and it is still an active research field. Modern approaches are comprehensively reviewed, e.g., in [20, 13]. Recently, with the advent of deep learning technology, there is an observed growing trend toward the application of artificial neural networks for semantic segmentation of the vascular system. Since it is also an area of interest in the current study, below some examples most relevant to our research are recalled. For the description of conventional approaches, which utilize vessel enhancement [6], template matching [28], region growing [1], or level-set methods [16, 8], the reader is referred to the provided citations.

A large part of published works concerns vessel segmentation in retinal images. For example, in [22] the authors employed a standard architecture of a convolutional neural network (CNN), with 3 convolutional layers, each followed by a max-pool operator, and then a head composed of two consecutive fully connected layers. The network input is a 61x61 pixel patch cropped from the original full-resolution OCT image and the output of the last, 2-neuron classification layer provides the probability estimate that the central patch pixel belongs either to a vessel or a background tissue. This kind of network is an example of architecture, where image pixels are classified based on the context embraced by an image patch. The effectiveness of such an approach is poor due to the need to iterate through multiple overlapping image patches, thus repeating the convolution operations for the same image regions. Nonetheless, such a methodology was utilized in a series of studies, also in the context of other organs and imaging modalities, e.g. liver (CT) [10], esophagus (NBI microscopy) [30], or carotid arteries (US) [24].

An extension to regular CNN architecture with a fully connected output classification layer is the Fully Convolutional Network (FCN) architecture. Instead of the fully connected layer, a tensor of deconvolution filters forms the FCN head, with each filter responsible for activating an individual pixel in the resulting segmentation mask. This mechanism allows for avoiding repeated processing of the overlapping image patches and provides finer delineation of the vessel walls. However, the output mask resolution is usually lower than that of the input image. FCN was reported to ensure satisfactory results in application

ICCS Camera Ready Version 2023
To cite this paper please use the final published version:
DOI: 10.1007/978-3-031-36027-5_20

to the segmentation of e.g. left ventricle vasculature [29], or cardiovascular and pulmonary vessels [17] in MRI and CT images.

Advances in encoder-decoder architectures resulted, on other hand, in numerous semantic segmentation network models. The most common architecture of this kind is the classic U-Net model [23], initially developed for segmenting neuronal structures in electron microscopic 2D images. In regard to vessel segmentation, this model was applied, e.g. to recognize retinal vessels in scanning laser ophthalmoscopy images [18], cerebral arteries in TOF-MR angiograms[14] or renal vasculature in CT data [27]. A 3-dimensional variant of U-Net was utilized in application to cerebral arteries also in TOF-MR angiograms [5].

Authors not only employ standard U-Net configuration with convolutional layers in both encoder and decoder paths with skip connections between the corresponding branch levels but also introduce custom modifications. For example, Wang et al. replace some of the convolution layers in the contracting path with ResNest blocks [9] to increase the saliency of the extracted image embeddings. Moreover, the skip connections which in the regular U-Net perform simple concatenation are enhanced by inserting the frequency channel attention (FCA) units between the encoding layers output and the corresponding decoder inputs. The role of the FCA blocks is to compensate for the potential mismatch between low- and high-level image features. A similar model is proposed in [4] for segmenting 3D coronary CTA images. Here the attention-guided modules fuse embeddings generated by adjacent levels of the encoder-decoder hierarchy to automatically capture the most relevant information inferred by the two paths. Moreover, the feature map on the output of the network bottleneck, before passing it on to the decoder, is processed by the scale-aware feature enhancement layer. This component extracts and selects image embeddings sensitive to various vessel scales. Eventually, the last layer of the decoder is formed by the multi-scale aggregation module, capable of adaptive fusing information from various decoder stages.

The fundamental challenge in any deep-learning task is preparing the representative training data set. The number of image-segmentation mask pairs should be large enough to cover the variability of the input domain. Apparently, according to the review presented in [13], the number of subjects involved in the DL experiments ranges from just a few scans up to several hundred. Hence, in most of the experiments, data augmentation techniques are involved to artificially increase the training set size to thousands of 2D images. In the study described in [7], more than 18 thousand scans were collected, but such big data sets are rather scarce, and usually not available for academic research groups. Therefore, some researchers postulate using synthetic data sets instead of real ones. Such approaches can be found in [26] and [29] where the image simulation procedures mimic CT and MR angiography, respectively. The intrinsic advantage of simulator-generated training examples is that ground-truth segmentation masks are automatically available, as the underlying vessel tree models are needed to synthesize the images. Thus, neither data annotation effort nor its quality check is required. In the published works, however, no study

ICCS Camera Ready Version 2023
To cite this paper please use the final published version:
DOI: 10.1007/978-3-031-36027-5_20

devoted explicitly to realistic contrast-enhance MR angiography is reported. In [29], where the coreMRI simulation platform [3] was utilized, only the 2D image slices were generated using a single-shot balanced steady-state free precession pulse sequence together with the 4D-XCAT whole-body anatomical model, from which the cardiac vasculature and tissue region was extracted.

2.2 Current contribution

Considering the above-presented state-of-the-art, there are three aspects that can be distinguished as potential fields of improvement. Firstly, for the need of vessel segmentation in contrast-enhanced MR angiography images, a dedicated data set must be collected. Similarly to other researchers, we postulate to create a database of simulated images. For that purpose, we extended our MR angiography simulation framework [12] to the contrast-enhanced acquisition method. Moreover, as we focus on the intracranial arterial system, we constructed a series of cerebral vascularity models both normally appearing as well as with various lesions, such as aneurysms and stenoses. Thus, in contrast to previous works which used arterial models synthesized according to vessel tree-growth simulation algorithms, our approach is based on realistic anatomies reconstructed from true patient data. Secondly, in order to better exploit the multi-scale nature of the vessel system, we introduce a custom modification of the V-Net's encoder path. In our model, the last extracted feature map is passed through the atrous spatial pyramid pooling block, as in the backbone of the DeepLabV3 architecture [2]. Our solution stems from the observation that features must be extracted at multiple scales on the initial steps of the processing path and not only at the decoder output so that all the subsequent decoding stages can reconstruct coarse and fine geometrical vessel details. Then, the multi-scale feature maps representing various levels of geometry are stacked and aggregated with the use of a GRU module. Thirdly, instead of expanding the network architecture with an attention mechanism, criticized for the increased computational cost attributed to the need of learning unimportant features, we propose to enrich the input context information by manually-engineered image embeddings. This task is realized by the vessel-enhancement block which contains a bank of filters sensitive to tubular structures [6].

3 Methods and materials

3.1 Vessel segmentation model

Base architecture. The objective of the current study was to develop an efficient vessel segmentation model that would incorporate multiscale image feature extraction and a robust mechanism to account for the global context of an imaged organ vasculature. For that purpose, we propose the architecture visualized in Figure 1. It is essentially based on the concept of V-Net—a volumetric fully convolutional network [19]. The main computational units in the encoder path

ICCS Camera Ready Version 2023
To cite this paper please use the final published version:
DOI: 10.1007/978-3-031-36027-5_20

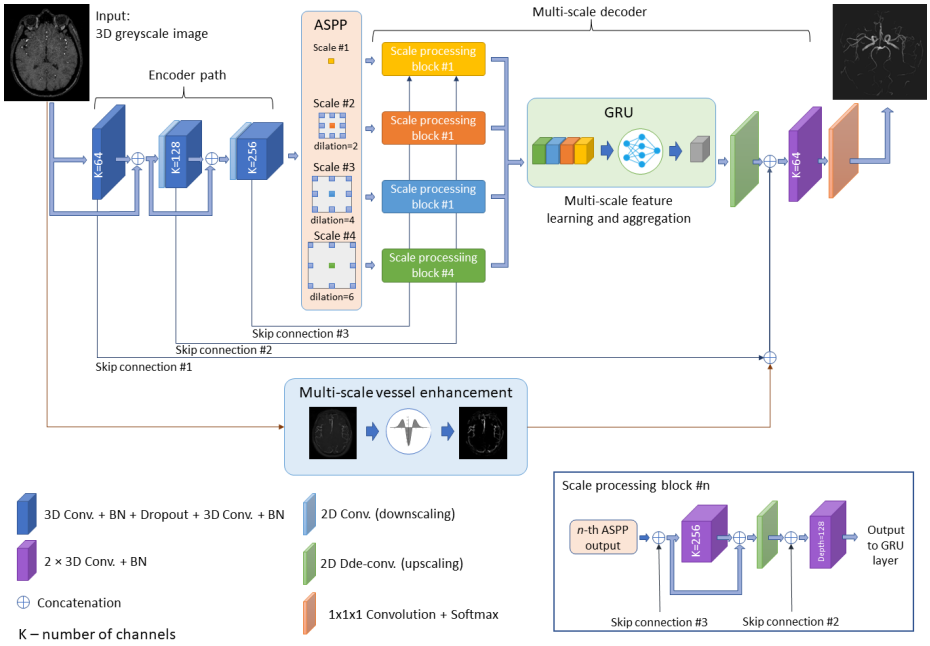

Fig. 1. Overview of the proposed vessel segmentation network architecture.

realize $5 \times 5 \times 5$ convolution with stride=1. At each stage, there are 2 convolution layers followed by batch normalization and dropout layer (with probability $p = 0.2$). The activation function for the convolutional layers is the parameterized ReLU. The number of filters in the first stage equals 64 for both layers and doubles in consecutive stages. As proposed in the original paper, the input to each stage is passed over and added to this stage's output, thus enabling the learning of a residual function and decreasing the convergence time. The resolution of image embedding maps is reduced after each stage by a convolution layer with $2 \times 2 \times 2$ kernel with stride 2. Eventually, the outputs of the contractive path stages are concatenated with the inputs of the corresponding blocks in the expansion path.

Multi-scale feature extraction and aggregation. The network embeddings extracted at the third stage of the encoder already comprise rich semantic information. Further reduction of the input resolution poses a risk of hiding varied geometrical patterns characteristic of vessels at different scales. Hence, instead of another contractive step, the proposed model contains the atrous spatial pyramid pooling block, which provides feature encoding at various scales and simultaneously leverages high-resolution context information around the vessels. We adopt the idea of ASPP blocks to 3 dimensions and use 4 kernels of sizes $1 \times 1 \times 1$ (pointwise), and $3 \times 3 \times 3$ with dilation rates r=2, 4, and 6.

ICCS Camera Ready Version 2023
To cite this paper please use the final published version:
DOI: 10.1007/978-3-031-36027-5_20

The feature maps extracted in the ASPP block are then propagated in 4 parallel paths through decoder convolution blocks (kernel size=$5 \times 5 \times 5$) and upscaling deconvolution ($2 \times 2 \times 2$, stride=2). Before reaching the last layer, these 4 feature maps are stacked in a sequence and aggregated using a 1-layer GRU block, which automatically selects embeddings relevant to segmentation on each scale.

Vessel-enhancement block. The trend toward discarding conventional image processing methods in favor of deep learning has led to the development of network architectures of sometimes unnecessarily high complexity. Although ultimate performance can be satisfactory, it is often attained at the increased training effort and the size of the model. Moreover, there is a risk of overfitting since the complex network does not attain the global context information and cannot generalize to new cases. Hence, we propose to enhance the contextual information by filtering the input image using a classic multi-scale vessel enhancement function [6]. It uses derivatives of Gaussian kernels to analyze local image contrast in various directions. In our implementation, we configure the enhancement procedure to five scales, i.e., values of the standard deviation of the probing Gaussian kernels, which were equal to 0.5, 1, 2, 4, and 8 mm. Such a filtered image is then concatenated with the aggregated output of the GRU unit and passed through the last convolution block. Finally, the output of the decoder is convolved channel-wise with the filter of size $1 \times 1 \times 1$. The obtained values are consumed by the soft-max function which generates the output segmentation mask. The network training is accomplished by minimizing the standard cross-entropy loss function.

3.2 MR angiography simulation

Cerebral arterial models. The input to the simulation algorithm, apart from the imaging parameters (such as sequence timing parameters, the field of view, etc.), is the model of the imaged organ. In the case of angiography simulation, the model comprises the geometry of the arterial tree, its functional description, i.e. blood flow through the vessel system, and the stationary tissue mimicking the perfusion volume. The first problem is therefore the reconstruction of a realistic arterial tree geometrical model.

We approach this challenge by manually annotating cerebral vessels in a high-resolution CE-MRA image. For the need of this study, we exploit the IXI dataset [15] - an open database containing 570 MRA images of healthy subjects. Since this study is a preliminary research directed toward the utilization of synthetic images for the training of deep-learning segmentation models, we selected a subset of 30 MRA volumes for the development of training examples. The in-plane resolution of the images was equal to 0.46875×0.46875 mm2 with the matrix size=512×512 pixels. The number of axial slices was 100 and the spacing between slices, as well as slice thickness, was equal to 0.8 mm.

Given the vessel system segmentation, its geometric description can be obtained. Firstly, in our algorithm, the segmentation mask is skeletonized to roughly

ICCS Camera Ready Version 2023
To cite this paper please use the final published version:
DOI: 10.1007/978-3-031-36027-5_20

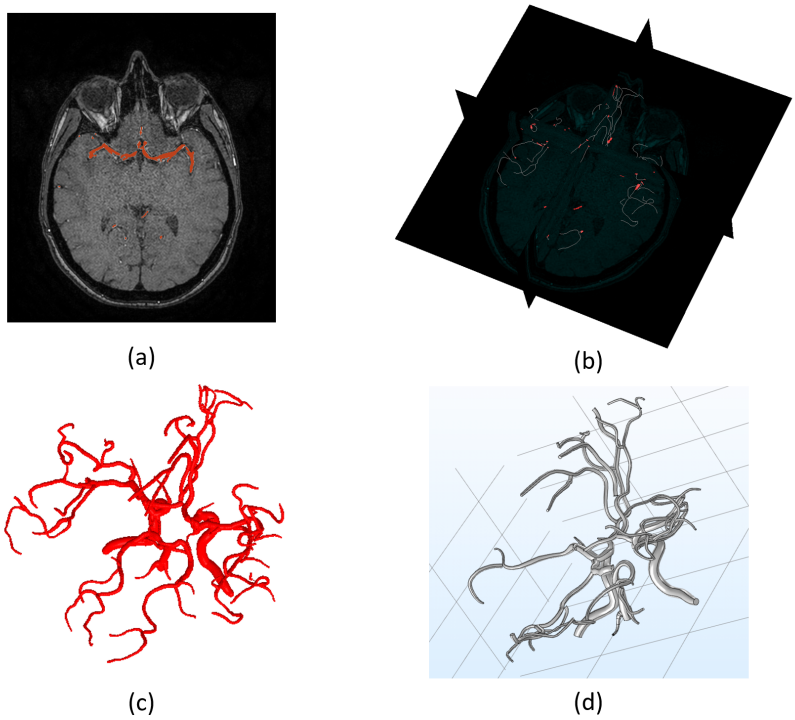

Fig. 2. Reconstruction of a cerebral arterial tree using VesselKnife and Comsol software. Manual annotation of arteries in the real CE-MRA volume (a). Skeletonization of the binary annotation mask and centerline determination (b). Radius estimation along the centerlines (c). Geometry reconstruction in the Comsol software to simulate the blood flow.

identify the courses of the vessel centerlines. These centerlines were defined on the discrete raster, hence they then must be smoothed to obtain a continuous description. The smoothing process involves minimizing the second derivatives calculated at the subsequent nodes of centerlines.

Next, the vessel radii are determined along the smoothed centerlines using the algorithm implemented in the *VesselKnife* software [25]. For a given node point on the centerline, a set of rays passing through that point is defined. The rays are led in multiple directions in order to equally penetrate the space around the node. The number of rays can be adjusted to the user's needs and it is a tradeoff between computational effort and precision of radius estimation. Each ray intersects the vessel wall which is determined as a boundary between white and black regions in the segmentation binary mask. The covariance matrix is then constructed for the distribution of the intersection points. The principal component decomposition of this covariance matrix indicates the local vessel orientation (component with the highest eigenvalue) and its radius, which is approximated as the square root of the smallest eigenvalue multiplied by 2.

ICCS Camera Ready Version 2023
To cite this paper please use the final published version:
DOI: 10.1007/978-3-031-36027-5_20

Figure 2 presents an example of the reconstructed cerebral arterial tree and the intermediate products of the reconstruction algorithm. Moreover, a vessel system directly obtained from the reconstruction can be modified to include abnormal structures, such as stenosis and aneurysms. The first malformation is obtained by locally decreasing a vessel radius, whereas saccular aneurysms are simulated by adding ellipsoidal objects linked with short vessel segments, as illustrated in Fig. 3.

MR simulation framework. In this study, we use our previously developed framework for MR angiography simulation [11]. Below, we briefly summarize only the main parts of the system. The first component models the blood flow in the vasculature of the imaged organ. For that purpose, we utilize the computational fluid dynamics (CFD) module available in the COMSOL Multiphysics software [28]. The Navier-Stokes equation is used to describe the blood flow, assuming a laminar regime, rigid vessel walls, constant viscosity, and incompressibility of the fluid. The output of CFD simulation is presented as a velocity vector field and flow streamlines. Then, within the MRI simulation module, the whole arterial tree is filled in with virtual particles mimicking blood isochromats. The particles are positioned along the streamlines and—to ensure that the fluid incompressibility assumption is kept—distributed relative to the velocity vector field. Thus, if velocity locally increases, as in a region of stenosis, the distances between the particles along the flow direction become larger. During the simulation process–which is essentially a time-dependent procedure—the particles move along the streamlines from the vessel tree inlet to its outlet terminals. Whenever a particle leaves its trajectory, it is replaced by a new one at that trajectory input node. The system keeps track of all particles and can determine their current locations with arbitrary temporal resolution. The number of streamlines and the number of particles positioned thereon depend on the size of the vasculature model.

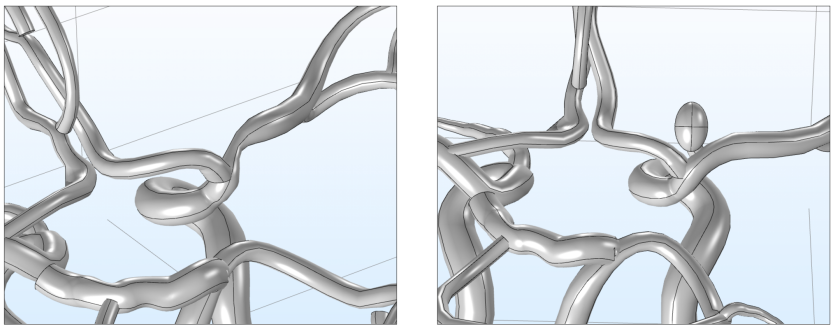

Fig. 3. Malformations introduced into normally-appearing arterial models: stenosis (a) and aneurysm (b) in a middle cerebral artery.

ICCS Camera Ready Version 2023
To cite this paper please use the final published version:
DOI: 10.1007/978-3-031-36027-5_20

Table 1. MRI parameter values used in experiments.

	ρ [%]		T_1 [msec]		T_2 [msec]	
Tissue type	μ	σ	μ	σ	μ	σ
Blood	100	-	200	10	50	5
Stationary	83	8	920	90	100	10

Based on our past experiments with non-contrast-enhanced sequences [11], we adjust the particle number to obtain the density of 15-20 particles per 1 mm^3.

From the vessel segmentation algorithm perspective, it is also important that the final image comprises also static tissue. Only then, the segmentation model can learn not only the geometry of the vessels but also the background context. Therefore, apart from moving particles located on vasculature streamlines, the simulated object is composed of stationary particles surrounding the arteries. Each particle is assigned magnetic parameters – proton density (ρ), longitudinal (T_1), and transverse (T_2) relaxation times. We set these parameters to values characteristic of the gadolinium-enhanced blood and gray matter in the field strength $B_0 = 1.5$ T. The parameter means and standard deviations used in the experiments under the current study are provided in Table 1. In order to achieve higher variability of the intensity patterns in the synthesized images, the exact values for a given object are randomly sampled from the Gaussian distribution.

The MRI simulation block handles the time passage and manages the imaging events, i.e. RF excitation pulses, phase, and frequency encoding gradients, as well as free precession stages. The specific events are switched on and off according to the prescribed acquisition method and the corresponding sequence parameters, i.e. echo and relaxation times (TE and TR), and the flip angle (FA). Similarly to object attributes, sequence parameters are randomly sampled using mean and standard deviation values, i.e. TR = 20 ($\sigma = 2$) msec, TE = 7 ($\sigma = 1.2$) msec, FA = 15($\sigma = 3$)°. The chosen parameter ranges correspond to the T_1-weighted spoiled gradient echo sequence, with which the CE-MRA acquisitions are routinely accomplished.

The magnetic vectors M_p of all spin isochromats associated with object particles p are initially aligned with the z-axis. At a given time t of the simulation, M_p vectors are flipped toward the transverse plane, and the new state after excitation is calculated as

$$M_p\left(t+\delta t\right) = R_{\mathrm{RF}}\left(\alpha_{\mathrm{eff}}\right) M_p\left(t\right), \tag{1}$$

where δt indicates the temporal resolution of the simulation, R_{RF} rotates M_p about the x-axis. α_{eff} is the effective flip angle that encapsulates off-resonance conditions causing changes in the assumed flip angle α.

The post-excitation evolution of the magnetization vectors is governed by the analytical solution to the Bloch equation as

$$M_p\left(t+\delta t\right) = Rot_z\left(\theta_g\right) Rot_z\left(\theta_i\right) R^{12}_{\mathrm{relax}} M_p\left(t\right) + R^{1}_{\mathrm{relax}} M_0, \tag{2}$$

ICCS Camera Ready Version 2023
To cite this paper please use the final published version:
DOI: 10.1007/978-3-031-36027-5_20

where Rot_z rotates M_p around the z-axis due to the phase or frequency encoding gradient (θ_g) and field inhomogeneity effect (θ_i), whereas R^{12}_{relax} and R^{1}_{relax} account for the transverse and longitudinal relaxation phenomena. Finally, signal acquisition is accomplished by integrating contributions from every particle p in the k-space:

$$s(t) = \sum\nolimits_{p=1}^{n_p} M_p(t)\,\boldsymbol{x} + j \sum\nolimits_{p=1}^{n_p} M_p(t)\,\boldsymbol{y}, \tag{3}$$

with n_p indicating the total number of particles. The readout window is partitioned into nx segments, which correspond to the size of k-space in the frequency encoding direction. During the intervals between these sampling steps, the magnetization vectors of blood particles evolve as they move. Once the readout window is completed, one line of k-space is filled in. After each TR cycle, the remnant transverse magnetization is numerically canceled out before issuing the next RF pulse to achieve the behavior of the spoiled gradient echo method. The final step involves performing an FFT transform on the collected k-space data to reconstruct the image. Before reconstructing the image, it is possible to add thermal noise with a user-defined standard deviation to the measured signal. In this study, we used three different levels of noise, which led to reconstructed images with signal-to-noise ratios (SNRs) of 5:1, 10:1, or 20:1.

4 Experimental results

4.1 Simulated training images

The arterial tree models designed in this study consisted of 40 to 60 branches and comprised, apart from multiple smaller vessels, the main cerebral arteries, such as basilar artery (BA), internal carotid arteries (ICA), posterior cerebral and communicating arteries, anterior cerebral arteries, anterior communicating artery, and middle cerebral arteries (MCA). The simulation of blood flow was driven by setting pressure values in the circulatory stems inlets (BA, left and right ICA) and all the outlets. The pressure difference was adjusted to the values reported in the study [40], where the flow distribution in a real subject was measured with the use of phase-contrast angiography.

Figure 4 presents cross-sections and maximum intensity projection of an example simulated image with added noise at the SNR level = 20:1. All simulated images were formed with the matrix size=256 × 256 and the number of slices=100. The number of sequence parameter combinations reached 100. Consequently, 3,000 volumes were simulated which represented 30 reconstructed normally-appearing cerebral arterial trees. For each imaging parameters combination, an arterial tree was randomly rotated about all three spatial axes by an angle drawn from the interval $(-15\circ; +15\circ)$, so that virtual acquisitions are effectively made at arbitrary orientations. Each tree was also modified to contain one kind of lesion – stenosis or aneurysm. This intervention resulted in another 3,000 synthesized images. The raw k-space data were then corrupted by the Gaussian

ICCS Camera Ready Version 2023
To cite this paper please use the final published version:
DOI: 10.1007/978-3-031-36027-5_20

white noise, hence, in addition to noise-free images, the simulated dataset comprised 3 noisy variants. Overall, there were 24,000 synthetic CE-MRA volumes available for training and validation.

4.2 Tests of the segmentation model

The test images were selected as another subset of the IXI Database, disjunctive from the training subset. The tests of the proposed network were conducted on 50 volumes, for which the ground-truth masks were manually annotated by an observer experienced in image processing and later verified by a radiologist. Then, in order to gain insight into the capability of the model with reference to conventional image processing methods, all test volumes were filtered by the aforementioned vessel enhancement algorithm (with the same set of filter scales) and segmented automatically using the level-set segmentation method. The segmentation results obtained by both level-set and our proposed model were compared against ground-truth masks using the intersection-over-union (IoU) metric, given as

$$IoU = \frac{\sum_{i=1}^{K} y_i \wedge y_i^{pred}}{\sum_{i=1}^{N} y_i \vee y_i^{pred}} \tag{4}$$

where K designates the number of voxels in a processed image and y_i^{pred} is the predicted voxel category. Here, categories are Boolean-valued and a voxel is labeled *True* if it belongs to the artery, *False* otherwise. The averaged results are presented in Table 2. It must also be noted that the performance of various

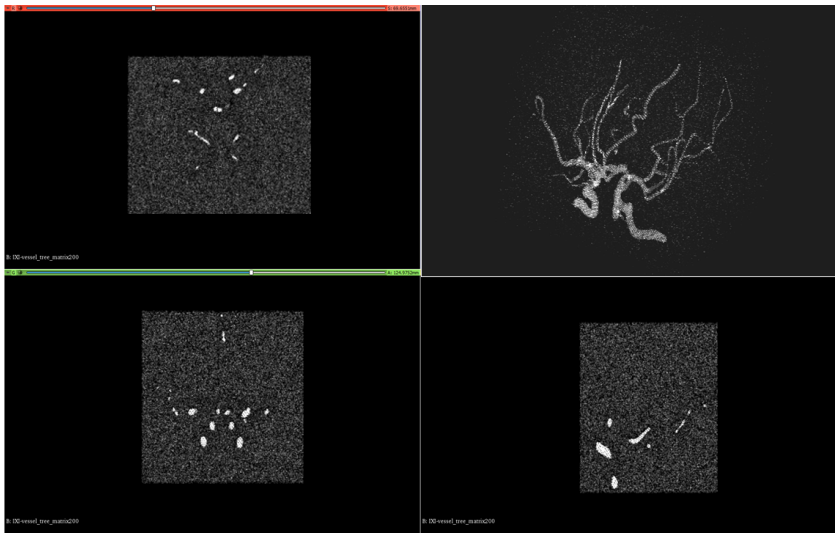

Fig. 4. Anatomical cross-sections and maximum intensity projection (upper-right) of an example simulated CE-MRA image.

ICCS Camera Ready Version 2023
To cite this paper please use the final published version:
DOI: 10.1007/978-3-031-36027-5_20

segmentation methods may differ with respect to the scale of a vessel. Hence, apart from reporting the overall mean IoU value, we investigated the behavior of both tested methods at 4 distinguished radii ranges of vessel segments.

5 Conclusions

To conclude, in this paper, we presented a novel architecture of a convolutional neural network specialized in the segmentation of cerebral arteries in CE-MRA images. We showed that it is feasible to obtain reasonable results using our network trained solely on synthetic data. The calculated IoU values are on average lower than the scores obtained with the use of the conventional level-set method. Apparently, however, the proposed network ensures better stability in terms of segmentation accuracy across various scales of vessel radii. This shows the potential of the designed multi-scale network configuration. In future works, we plan to improve the generalization capability of our model by conducting the training on a dataset reconstructed from a larger and more varied sample of MRA volumes.

When referred to other published studies, the obtained IoU ratios are in accordance with the state-of-the-art results in the domain of cerebrovascular segmentation—see Table 3. To enable comparison of the metrics calculated within the current contribution, the Dice coefficients (or F1-scores) reported in other papers were converted to IoU. As it can be seen, our segmentation model, although applied to a different imaging modality, performs either better or at a similar level than approaches proposed in [5] and [26]. On the other hand, the solution described in [31] achieved higher accuracy over all others. It must be noted, however, that their experiments involved significantly smaller training and test datasets, composed of only 109 ToF-MRA volumes.

References

1. Cetin, S., Unal, G.: A higher-order tensor vessel tractography for segmentation of vascular structures. IEEE Trans. on Medical Imaging **34**(10), 2172–2185 (2015)
2. Chen, L.C., Papandreou, G., Schroff, F., Adam, H.: Rethinking atrous convolution for semantic image segmentation (2017), https://arxiv.org/abs/1706.05587
3. CoreMRI: Advanced MR simulations on the cloud (2023), https://www.coremri.com/ (accessed March 3, 2023)

Table 2. IoU values obtained for the reference method and the proposed model.

Segmentation method	All radii	$r \leq 1$	$1 < r \leq 1.5$	$1.5 < r \leq 2$	$r > 2$
Level-set [16]	0.79	0.62	0.64	0.83	0.89
Proposed	0.75	0.72	0.73	0.76	0.77

r – vessel radius [mm]

ICCS Camera Ready Version 2023
To cite this paper please use the final published version:
DOI: 10.1007/978-3-031-36027-5_20

Table 3. Comparison of the obtained segmentation results with previous research.

Source	Modality	Architecture	IoU
Fan et al. [5]	ToF-MRA	3D U-Net / HMRF*	0.66
Tetteh et al. [26]	ToF-MRA	3D FCN / cross-hair conv.	0.76
Zhang et al. [31]	ToF-MRA	Dilated Dense CNN	0.95
Nazir et al. [21]	CTA	3D FCN / Inception	0.83
Current study	CE-MRA	3D V-Net / Vessel enhancement	0.75

* – hidden Markov random fields

4. Dong, C., Xu, S., Dai, D., Zhang, Y., Zhang, C., Li, Z.: A novel multi-attention, multi-scale 3d deep network for coronary artery segmentation. Medical Image Analysis **85**, 102745 (2023)
5. Fan, S., Bian, Y., Chen, H., Kang, Y., Yang, Q., Tan, T.: nsupervised cerebrovascular segmentation of tof-mra images based on deep neural network and hidden markov random field model. Frontiers in Neuroinformatics **13** (2020)
6. Frangi, A.F., Niessen, W.J., Vincken, K.L., Viergever, M.A.: Multiscale vessel enhancement filtering. In: Wells, W.M., Colchester, A., Delp, S. (eds.) Medical Image Computing and Computer-Assisted Intervention — MICCAI'98. pp. 130–137. Springer Berlin Heidelberg (1998)
7. Fu, F., Wei, J., Zhang, M., Yu, F., Xiao, Y., Rong, D., Shan, Y., Li, Y., Zhao, C., Liao, F., Yang, Z., Li, Y., Chen, Y., Wang, X., Lu, J.: Rapid vessel segmentation and reconstruction of head and neck angiograms using 3d convolutional neural network. Nature Communications **11**(1), 4829 (2020)
8. Gao, X., Uchiyama, Y., Zhou, X., Hara, T., Asano, T., Fujita, H.: A fast and fully automatic method for cerebrovascular segmentation on time-of-flight (tof) mra image. Journal of Digital Imaging **24**(4), 609–625 (2011)
9. He, K., Zhang, X., Ren, S., Sun, J.: Deep residual learning for image recognition (2015), https://arxiv.org/abs/1512.03385
10. Kitrungrotsakul, T., Han, X.H., Iwamoto, Y., Lin, L., Foruzan, A.H., Xiong, W., Chen, Y.W.: Vesselnet: A deep convolutional neural network with multi pathways for robust hepatic vessel segmentation. Computerized Medical Imaging and Graphics **75**, 74–83 (2019)
11. Klepaczko, A., Materka, A., Szczypiński, P., Strzelecki, M.: Numerical modeling of mr angiography for quantitative validation of image-driven assessment of carotid stenosis. IEEE Transactions on Nuclear Science **62**(3), 619–627 (2015)
12. Klepaczko, A., Szczypiński, P., Deistung, A., Reichenbach, J.R., Materka, A.: Simulation of mr angiography imaging for validation of cerebral arteries segmentation algorithms. Computer Methods and Programs in Biomedicine **137**, 293–309 (2016)
13. Li, H., Tang, Z., Nan, Y., Yang, G.: Human treelike tubular structure segmentation: A comprehensive review and future perspectives. Computers in Biology and Medicine **151**, 106241 (2022)
14. Livne, M., Rieger, J., Aydin, O.U., Taha, A.A., Akay, E.M., Kossen, T., Sobesky, J., Kelleher, J.D., Hildebrand, K., Frey, D., Madai, V.I.: A u-net deep learning framework for high performance vessel segmentation in patients with cerebrovascular disease. Frontiers in Neuroscience **13** (2019)

ICCS Camera Ready Version 2023
To cite this paper please use the final published version:
DOI: 10.1007/978-3-031-36027-5_20

15. London, I.C.: Brain Development (2023), https://brain-development.org/ixi-dataset/ (accessed March 3, 2023)
16. Manniesing, R., Velthuis, B., van Leeuwen, M., van der Schaaf, I., van Laar, P., Niessen, W.: Level set based cerebral vasculature segmentation and diameter quantification in ct angiography. Medical Image Analysis **10**(2), 200–214 (2006)
17. Merkow, J., Marsden, A., Kriegman, D., Tu, Z.: Dense volume-to-volume vascular boundary detection. In: Medical Image Computing and Computer-Assisted Intervention - MICCAI 2016. pp. 371–379. Springer International Publishing (2016)
18. Meyer, M.I., Costa, P., Galdran, A., Mendonça, A.M., Campilho, A.: A deep neural network for vessel segmentation of scanning laser ophthalmoscopy images. In: Image Analysis and Recognition. pp. 507–515. Springer Internl. Pub. (2017)
19. Milletari, F., Navab, N., Ahmadi, S.: V-net: Fully convolutional neural networks for volumetric medical image segmentation. In: 2016 Fourth International Conference on 3D Vision (3DV). pp. 565–571. IEEE Comp. Soc. (2016)
20. Moccia, S., De Momi, E., El Hadji, S., Mattos, L.S.: Blood vessel segmentation algorithms — review of methods, datasets and evaluation metrics. Computer Methods and Programs in Biomedicine **158**, 71–91 (2018)
21. Nazir, A., Cheema, M.N., Sheng, B., Li, H., Li, P., Yang, P., Jung, Y., Qin, J., Kim, J., Feng, D.D.: Off-enet: An optimally fused fully end-to-end network for automatic dense volumetric 3d intracranial blood vessels segmentation. IEEE Transactions on Image Processing **29**, 7192–7202 (2020)
22. Prentašić, P., Heisler, M., Mammo, Z., Lee, S., Merkur, A., Navajas, E., Beg, M.F., Šarunic, M., Lončarić, S.: Segmentation of the foveal microvasculature using deep learning networks. Journal of Biomedical Optics **21**(7), 075008 (2016)
23. Ronneberger, O., Fischer, P., Brox, T.: U-net: Convolutional networks for biomedical image segmentation. In: LNCS. vol. 9351, pp. 234–241 (10 2015)
24. Smistad, E., Løvstakken, L.: Vessel detection in ultrasound images using deep convolutional neural networks. In: Deep Learning and Data Labeling for Medical Applications. pp. 30–38. Springer International Publishing (2016)
25. Szczypiński, P.: VesselKnife (2023), http://eletel.p.lodz.pl/pms/SoftwareVesselKnife.html (accessed March 3, 2023)
26. Tetteh, G., Efremov, V., Forkert, N.D., Schneider, M., Kirschke, J., Weber, B., Zimmer, C., Piraud, M., Menze, B.H.: Deepvesselnet: Vessel segmentation, centerline prediction, and bifurcation detection in 3-d angiographic volumes. Frontiers in Neuroinformatics **14** (2020)
27. Wang, C., Roth, H.R., Kitasaka, T., Oda, M., Hayashi, Y., Yoshino, Y., Yamamoto, T., Sassa, N., Goto, M., Mori, K.: Precise estimation of renal vascular dominant regions using spatially aware fully convolutional networks, tensor-cut and voronoi diagrams. Computerized Medical Imaging and Graphics **77**, 101642 (2019)
28. Worz, S., Rohr, K.: Segmentation and quantification of human vessels using a 3-d cylindrical intensity model. IEEE Trans. on Image Proc. **16**(8), 1994–2004 (2007)
29. Xanthis, C.G., Filos, D., Haris, K., Aletras, A.H.: Simulator-generated training datasets as an alternative to using patient data for machine learning: An example in myocardial segmentation with mri. Computer Methods and Programs in Biomedicine **198**, 105817 (2021)
30. Xue, D.X., Zhang, R., Feng, H., Wang, Y.L.: Cnn-svm for microvascular morphological type recognition with data augmentation. Journal of Medical and Biological Engineering **36**(6), 755–764 (2016)
31. Zhang, B., Liu, S., Zhou, S., Yang, J., Wang, C., Li, N., Wu, Z., Xia, J.: Cerebrovascular segmentation from tof-mra using model- and data-driven method via sparse labels. Neurocomputing **380**, 162–179 (2020)

ICCS Camera Ready Version 2023
To cite this paper please use the final published version:
DOI: 10.1007/978-3-031-36027-5_20